JOURNAL OF CATALYSIS 81, 358–368 (1983)

Identification of a Weak Adsorption State of Carbon Monoxide on Highly Dispersed, Alumina-Supported Platinum

RICHARD K. HERZ AND DAVID F. MCCREADY

Physical Chemistry Department, General Motors Research Laboratories, Warren, Michigan 48090

Received October 5, 1982

Temperature-programmed desorption of CO from 0.1 wt% Pt/Al_2O_3 was measured as a thin wafer of the material was heated in vacuum. At a Pt dispersion of 100% (CO/Pt = 0.92), a relatively tall, narrow CO desorption peak was obtained at low temperatures (355 K at 0.93 K s^{-1}) followed by a low, broad desorption band extending to 750 K. As the Pt dispersion decreased to 80% (CO/Pt = 0.70) and then 70% (CO/Pt = 0.64) as a result of pretreatment in O_2 and H_2, the fraction of CO that desorbed in the low-temperature peak decreased and the fraction of CO that desorbed in the broad desorption band increased. At Pt dispersions below 40%, only a broad desorption band was obtained, a result which is in agreement with data reported by others. The low-temperature peak is interpreted as desorption of CO from very small Pt particles (<20 atoms, <1.1 nm) supported on transitional Al_2O_3. The broad desorption band is interpreted as CO desorption from larger Pt particles. Results from experiments performed at different heating rates indicate that the enthalpy of CO adsorption in the state that corresponds to the low-temperature peak is 74 ± 4 kJ mol^{-1}, an adsorption energy which is lower than energies obtained from measurements of CO desorption from Pt single crystal surfaces.

INTRODUCTION

The technique of temperature-programmed desorption, or thermal desorption, has been used to provide quantitative measurements of the bond energies between CO and adsorption sites on the surfaces of Pt single crystals. Although the technique has been applied in several instances (*1–6*) to the study of CO chemisorption on Pt that is dispersed over porous supports, there has been no quantitative analysis of the desorption data for two reasons. One reason is that most of the temperature-programmed desorption (TPD) curves that have been measured do not show well-resolved peaks corresponding to desorption from discrete CO–Pt adsorption sites. The second reason is that the quantitative analysis of TPD results obtained with porous adsorbents is complicated by the possible presence of competition between adsorption and desorption during an experiment. In a previous report (*1*) we have shown that CO adsorption will compete with desorption to the extent that adsorption equilibrium is closely approached during TPD of CO from porous Pt/Al_2O_3. In this report we (1) describe a novel experimental TPD apparatus, (2) present results for the TPD of CO from porous Pt/Al_2O_3 with different Pt dispersions, and (3) identify a well-resolved, low-temperature TPD peak over highly dispersed Pt.

The narrow width of the low-temperature TPD peak indicates that the corresponding adsorption state chemisorbs CO with a relatively uniform bond energy. Quantitative analysis of heating-rate-variation experiments shows that this adsorption state chemisorbs CO weakly relative to CO adsorption over less well-dispersed supported Pt and bulk Pt metal. Our identification of the low-temperature TPD peak and its corresponding weak CO adsorption state confirms the qualitative observations of Roth-

0021-9517/83 $3.00

schild and Yao (*7*). Their "outgassing" experiments and related work by Poppa and co-workers (*8, 9*) with metal on nonporous supports are considered in relation to our results in the Discussion section.

EXPERIMENTAL

Materials

The 0.1-wt% Pt/Al_2O_3 was prepared by impregnation of granules 0.12–0.15 mm in size of high purity transitional Al_2O_3 (110 m^2 g^{-1}, Davison Chemical Co.) to incipient wetness with aqueous H_2PtCl_6. After drying in air at ambient temperature for 3 h and in a vacuum oven at 393 K for 16 h, the sample was heated in flowing dry air at 773 K for 3 h and then in flowing wet air (air flowed through a bubbler at ambient temperature) at 773 K for 20 h. The 1.0-wt% Pt/Al_2O_3 was impregnated and dried by the same procedure, and then heated in flowing dry air at 773 K for 4 h. Pt loadings were confirmed by atomic absorption spectroscopy. Granules of Pt/Al_2O_3 were ground to powder before sample wafers were pressed.

High purity O_2 (99.995%) and H_2 (99.999%) were used to pretreat Pt/Al_2O_3 samples. O_2 flowed through a Drierite trap and a zeolite trap, and H_2 flowed through an Oxisorb cartridge (Analabs, Inc.). CO (93% ^{13}CO, 7% ^{12}CO; Merck, Inc.) was contained in a glass bulb.

Apparatus

A schematic diagram of the apparatus is shown in Fig. 1. A sample in the form of a rectangular wafer is located in a 7.4-mm i.d. quartz tube and is heated by radiation from two tungsten lamps. For the limiting case in which all radiation is absorbed by the outer surface of a sample, we estimate that temperature gradients within the sample are negligible (<0.1 K) at the heating rates used here (0.21–2.4 K s^{-1}).

A wafer is prepared by pressing sample powder around a bare chromel–alumel thermocouple (0.05-mm diameter wires). The

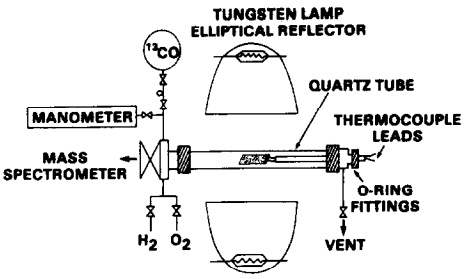

FIG. 1. Schematic of the apparatus used to measure the temperature-programmed desorption (TPD) of CO from porous Pt/Al_2O_3 into vacuum. Sample powder is pressed around a fine thermocouple into the form of a thin wafer. The sample is pretreated in atmospheric-pressure O_2 and H_2 before adsorption of ^{13}CO. Radiation from tungsten lamps is used to heat the sample in the evacuated quartz tube, and CO desorbs and is measured by a mass spectrometer.

0.1-wt% Pt/Al_2O_3 wafer was 11.6 mm long, 6.0 mm wide, and 0.17 mm thick; it weighed 14 mg (not including thermocouple) and contained about 15,000 cm^2 of Al_2O_3 surface and 40 cm^2 of Pt surface. The fine thermocouple wires protruding from a wafer are spot-welded to 0.25-mm diameter wires of the same composition. A wafer is supported by the thermocouple leads on one end and contact between its corners and the quartz tube on the other end. The 0.25-mm thermocouple leads pass through a 2 hole, 3.2-mm o.d. alumina insulator to connections outside the quartz tube. High vacuum epoxy seals the holes in the end of the alumina insulator that is located outside of the quartz tube. O-ring fittings are used to make vacuum-tight connections between the quartz tube, the alumina insulator, and the rest of the system.

A 15-mm i.d. right-angle valve connects the quartz TPD cell to a vacuum chamber which houses a quadrupole mass spectrometer. The chamber is pumped by a liquid-nitrogen-trapped diffusion pump and has a base pressure in the low 10^{-7}-Pa range. The TPD cell also has connections which allow pretreatment of a sample in flowing atmospheric-pressure H_2 and O_2, dosing of the sample with CO, and rough evacuation of the cell by a rotary pump through a liquid-

nitrogen-cooled trap and a zeolite trap (rough-vacuum line not shown in Fig. 1). The glass bulb filled with ^{13}CO is connected through two valves to the TPD cell. A sample is dosed by first filling the short line between the two valves with CO and then expanding this gas into the cell. A capacitance manometer measures the pressure in the cell during dosing of the sample.

The time constants which characterize the rate of accumulation of gaseous CO in the TPD cell and in the vacuum chamber by flow of CO were determined to be 0.04 and 0.3 s, respectively. The values of these time constants are small with respect to the times over which changes in net CO desorption rates occurred during our TPD experiments. Thus, the changes in net CO desorption rates we measured were determined only by processes occurring within the sample, that is, our TPD curves were not distorted by "flow lags" in the TPD cell or the vacuum chamber. The time constant of the TPD cell was estimated by dividing the measured volume of the cell (34 cm^3) by the calculated conductance of the quartz tube for CO at 300 K (800 cm^3 s^{-1}). The time constant of the vacuum chamber was determined by measuring the exponential response of the concentration of N_2 in the chamber following the rapid opening and closing of a piezoelectric leak valve. The volumetric flow rate (pumping speed) from the chamber was determined to be 1.3×10^4 cm^3 s^{-1} by dividing the measured volume of the chamber (4×10^3 cm^3) by the time constant.

A microcomputer is interfaced to the sample thermocouple, the programmable DC supply that powers the heating lamps, and the mass spectrometer. During a TPD experiment, the computer increases the power supplied to the heating lamps, records the sample temperature, scans preselected quadrupole mass/charge settings, and records the signals at these settings. The mass spectrometer signal is processed by a logarithmic amplifier before being read by the computer's 12-bit A/D converter; this procedure provides better than 1% resolution of changes in mass peak heights over a wide range of peak heights.

A reference leak of N_2 is used to set the sensitivity of the mass spectrometer to a constant level before each experiment. The response of the spectrometer to CO was determined by recording and integrating the mass 29(28) signal obtained by desorption of $^{13}CO(^{12}CO)$ from a 1-wt% Pt/Al_2O_3 wafer of known weight. The CO chemisorption capacity of the Pt/Al_2O_3 had been determined previously in a volumetric chemisorption apparatus, so the integrated mass spectrometer signal (V s) could be related to a known quantity of CO (mol). We then determined the relationship between the instantaneous signal (V) and the CO concentration in the vacuum chamber (mol cm^{-3}) by making the assumption that the response of the mass spectrometer is linear and by dividing the amount of CO that was desorbed in the calibration experiment (mol) by the volumetric flow rate from the chamber (cm^3 s^{-1}).

Procedure

At the start of a set of TPD experiments, the 0.1-wt% Pt/Al_2O_3 sample was given pretreatments in O_2 (to remove carbonaceous deposits) and H_2 (to remove oxygen). First a flow of atmospheric-pressure O_2 was started through the cell and the sample temperature was increased at a rate of 0.33 K s^{-1} to 773 K. After 0.5 h at 773 K in O_2, the cell was evacuated and the sample was allowed to cool rapidly to ambient temperature. Next a flow of atmospheric-pressure H_2 was started, and the sample temperature was increased at 0.33 K s^{-1} to 573 K. After 1 h at 573 K in H_2, conditions sufficient to remove all oxygen from Al_2O_3-supported Pt (*10*), the cell was evacuated and the sample temperature was increased at 1 K s^{-1} to 793 K. The sample was degassed in vacuum for 1 h at 793 K and then allowed to cool rapidly to ambient temperature.

At the start of a TPD experiment, the sample was saturated with CO at ambient

temperature by expanding CO into the cell to a pressure of 2.9 kPa (22 Torr). The CO was then pumped out through the rough-vacuum line and the cell was opened to the mass spectrometer chamber. We found that our results were insensitive to changes in the dosing pressure, the length of time CO was exposed to the sample, and the evacuation time. Signals at the following mass/charge ratios were recorded during each experiment as the sample was heated: 2, 18, 28, 29, 44, and 45. These mass settings were chosen to follow the desorption of H_2, H_2O, ^{12}CO, ^{13}CO, $^{12}CO_2$, and $^{13}CO_2$, respectively. No desorption of H_2 or H_2O was detected during the experiments reported here. Mass/charge ratios 15 and 32 were also monitored during some experiments; however, no changes in signal were detected at these mass settings (i.e., no desorption of CH_4 or O_2).

Using the mass spectrometer calibration, we determined the molar concentration of CO that was present in the mass spectrometer chamber as a function of time during a TPD experiment. The product of the CO concentration in the chamber (mol cm^{-3}) and the volumetric flow rate from the chamber (cm^3 s^{-1}) equals the molar flow rate of CO from the TPD cell (mol s^{-1}). The ratio of the molar flow rate of CO to the estimated volumetric flow rate from the cell at 300 K (cm^3 s^{-1}) equals the estimated CO concentration in the cell, C_{co}^{ref} (mol cm^{-3}). TPD results are presented below as plots of C_{co}^{ref} versus time. Strictly, C_{co}^{ref} only approximates the actual concentration when the temperature of the CO in the cell remains at 300 K. Although the temperatures of the quartz tube and the enclosed CO increase to unknown extents during an experiment, C_{co}^{ref} is characteristic of the actual CO concentration that was established over the sample, and the product of C_{co}^{ref} and the estimated flow rate from the cell equals the measured net rate of CO desorption from the sample. Numerical simulations performed with modifications of the mathematical model we have described previously (*1*) demonstrate that the temperature of the CO surrounding a sample wafer does not affect the shapes or positions (with respect to time and sample temperature) of TPD peaks.

RESULTS

CO Desorption from Blank Al_2O_3

The amount of CO that desorbs from the transitional Al_2O_3 is less than 10% of the amount of CO that desorbs from the 0.1-wt% Pt/Al_2O_3 after both materials have been degassed at 793 K and dosed with CO at ambient temperature (standard procedure). CO desorbs from the Al_2O_3 in a narrow peak with a maximum at 361 K at a heating rate of 1 K s^{-1}.

CO_2 Desorption

The amount of CO_2 that desorbed from 0.1-wt% Pt/Al_2O_3 following dosing with CO was about 20% of the amount of CO that desorbed. The source of this CO_2 was residual $^{12}CO_2$ in the TPD cell and $^{12}CO_2$ and $^{13}CO_2$ impurities in the CO bulb that adsorbed on the Al_2O_3. Observations which support this statement will be discussed here in some detail to answer questions about the possibility of CO_2 formation by CO dissociation and disproportionation.

First, the ratio of $^{12}CO_2$ to $^{13}CO_2$ was 3.0 during CO TPD, whereas the ratio of ^{12}CO to ^{13}CO was 0.08. A comparison of these ratios shows that most of the $^{12}CO_2$ that desorbed could not have been formed by reaction of CO but must have come from residual $^{12}CO_2$ in the cell and/or impurities in the CO bulb. Second, the result that the same amount of CO_2 desorbed from blank Al_2O_3, 0.1-wt% Pt/Al_2O_3, and 1-wt% Pt/Al_2O_3 following dosing with CO indicates that Pt was not involved.

Third, both the $^{12}CO_2$ and the $^{13}CO_2$ desorption curves measured over Pt/Al_2O_3 during CO TPD experiments look like the CO_2 desorption curve measured after deliberate CO_2 adsorption on blank Al_2O_3: a curve peaking at 375 K and tailing off grad-

ually at higher temperatures. This means that if CO_2 were formed by reaction of CO, the reaction must have occurred below 375 K. CO dissociation and disproportionation are not likely to occur over Pt below 375 K. In addition, these reactions deposit carbon which would have decreased the amount of CO adsorbed and desorbed in successive TPD experiments (*11*); however, we did not observe a decrease in CO desorption during successive experiments. Oxidation of CO by H_2O adsorbed on Al_2O_3 results in CO_2 formation and desorption over a temperature range substantially higher than the range over which we have measured CO_2 desorption during TPD of CO (*2*).

All of these observations support the conclusion that adsorption by Al_2O_3 of residual $^{12}CO_2$ in the cell and of $^{12}CO_2$ and $^{13}CO_2$ impurities in the CO bulb was responsible for the CO_2 desorption that we observed over Pt/Al_2O_3 during CO TPD experiments. We were not able to detect the CO_2 impurities in the CO bulb directly with the mass spectrometer. The relatively strong adsorption of CO_2 on Al_2O_3 (*12*) and the high surface area ratio of Al_2O_3 to Pt (about 370 for the 0.1-wt% Pt/Al_2O_3) are the probable reasons that the ratio of CO_2 to CO during TPD is greater than the ratio present in the CO bulb.

CO Desorption from Pt/Al_2O_3

Figure 2 presents the results of three experiments performed with one 0.1-wt% Pt/Al_2O_3 sample: curve 1 was obtained after one O_2–H_2 pretreatment, curve 2 was obtained after two pretreatments and intervening TPD experiments, and curve 3 was obtained after three pretreatments and intervening TPD experiments. The CO concentration in the TPD cell over the external surface of the sample is plotted versus time in the figure. The scale on the right hand side of the plot gives the equivalent pressure of CO in the cell (1 Torr = 133 Pa), and the scale on the top of the plot gives the sample temperature. All three experiments were performed under the same experimental conditions; the rate of increase in sample temperature was 0.93 K s^{-1}.

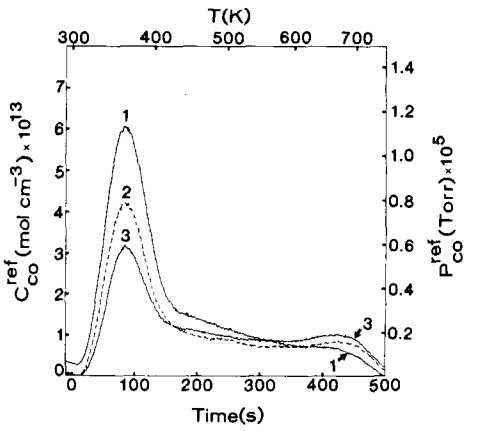

FIG. 2. Experimental measurements of the TPD of CO from 0.1-wt% Pt/Al_2O_3 at a heating rate of 0.93 K s^{-1}. The sample wafer was 0.17 mm thick and weighed 14 mg. The C_{co}^{ref} and P_{co}^{ref} are estimated concentration and equivalent pressure of CO over the external surface of the sample and are directly proportional to the measured net rate of CO desorption. The ratio of the total number of CO molecules adsorbed and desorbed to the total number of Pt atoms in the sample was 0.92 for curve 1, 0.70 for curve 2, and 0.64 for curve 3.

In each of the experiments, a relatively narrow, well-defined peak was obtained at low temperatures followed by a low, broad plateau or desorption band. The maxima of the low-temperature peaks are located at 355 K. The CO pressure over the external surface of the sample at the top of the peak in curve 1 was 1.1×10^{-5} Torr. At the same point, numerical simulations of the experiment indicate that the CO pressure at the center of the wafer was higher (about 10^{-3} Torr) as a result of the limited rate of CO diffusion out of the wafer.

The product of the area under a curve and the estimated volumetric flow rate from the cell equals the amount of CO that desorbed during the experiment. Note that one effect of an O_2–H_2 pretreatment was to reduce the amount of CO that desorbed in the subsequent TPD experiment. In addition to the experiments shown in Fig. 2, other TPD experiments, at the same heating rate and at higher and lower heating

rates, were performed following each pretreatment. The results obtained during up to six successive TPD experiments performed between two pretreatments were essentially identical, differing by no more than a few percent in both desorption rate at a given time and the total quantity of CO desorbed. This reproducibility indicates that CO could be adsorbed and desorbed repeatedly without deactivation of the sample, for example, by carbon deposition from disproportionation of CO or decomposition of trace hydrocarbons.

Since no deactivation of the sample occurred during an experiment, the number of CO molecules desorbed equals the number of CO molecules adsorbed initially and not removed by evacuation. The caption of Fig. 2 lists, for each experiment, the ratio (CO/Pt) of the number of adsorbed CO molecules to the total number of Pt atoms in the sample wafer. Under the assumption that Pt was not poisoned during the pretreatments, the changes in the CO/Pt ratios indicate that the pretreatments caused an increase in the average size of the Pt particles in the sample and a resulting decrease in the fraction of Pt atoms that were exposed on the surfaces of the particles. The maximum number of CO molecules that adsorb per surface Pt atom has been determined to be 0.87 ± 0.07 (*10, 13, 14*) for supported Pt particles with average sizes smaller than 5 nm. (The CO/surface Pt ratio decreases to about 0.5 for larger supported Pt particles, i.e., for Pt dispersions <20%, *14*). Dividing our CO/*total* Pt ratios by this CO/*surface* Pt ratio, we estimate that the percentage exposed or dispersion of the Pt was 100% (curve 1), 80% (curve 2), and 70% (curve 3) during the experiments shown in Fig. 2.

As the CO/Pt ratio decreased, the amount of CO that desorbed in the well-defined low-temperature peak decreased and the amount of CO that desorbed at times greater than 350 s (600 K) increased. When the curves in Fig. 2 are scaled so that they have the same area, curve 3 lies below curve 1 between 0 and 157 s (300–420 K) and lies above curve 1 at times greater than 157 s. Curve 2 crosses above curve 1 at 233 s (485 K). These comparisons indicate that, as the Pt dispersion decreased, the fraction of CO that desorbed in the low-temperature peak decreased and the fraction of the CO that desorbed in the broad desorption band increased.

Changes in the chloride content of the sample or incomplete reduction of the Pt were not responsible for the behavior we have observed. The chloride contents of two separate portions of the 0.1-wt% Pt/Al_2O_3, one given one O_2–H_2 pretreatment and one given three pretreatments, were both 0.07 wt%. The infrared spectrum of CO adsorbed on the 0.1-wt% Pt/Al_2O_3 was characteristic of reduced, supported Pt.

We have also performed TPD experiments with 1.0-wt% Pt/Al_2O_3 of varying dispersion and have obtained results similar to those for the 0.1-wt% sample. Over a 0.37-mm-thick 1.0-wt% Pt/Al_2O_3 wafer with high Pt dispersion, the low-temperature peak is broader and the peak maximum occurs at a higher temperature than over the 0.17-mm-thick 0.1-wt% wafer. The width of the peak at half height is 125 K over the 1.0-wt% sample and 75 K over the 0.1-wt% sample. The peak maximum occurs at 407 K over the 1.0-wt% sample and at 355 K over the 0.1-wt% sample. This broadening and shift of the peak is an expected result of the interaction between CO diffusion, adsorption, and desorption (*1*) and probably does not reflect differences in the intrinsic adsorption properties of the Pt.

At Pt dispersions below 40%, we do not observe a well-resolved low-temperature desorption peak. This result is in agreement with the data of Foger and Anderson (*2*) for CO desorption from a 0.9-wt% Pt/Al_2O_3 sample with a Pt dispersion of 40%. (They measured an H/Pt ratio of 0.42 by H_2 chemisorption, a CO/Pt ratio of 0.35, and an *average* Pt particle size of 2.3 ± 0.5 nm by electron microscopy.) In Fig. 3 we compare the TPD data reported by Foger and Anderson for desorption into flowing He (dashed

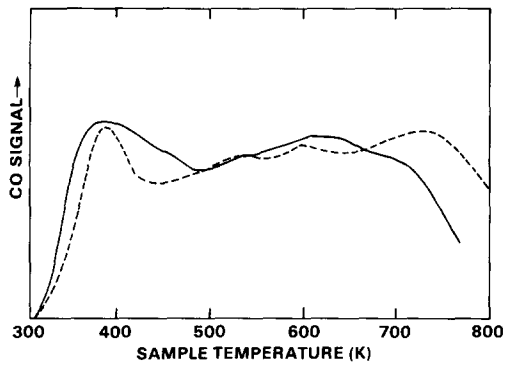

FIG. 3. Dashed curve: data of Foger and Anderson (*2*) for TPD of CO into flowing He from 0.9-wt% Pt/Al_2O_3 with a Pt dispersion of 40%; the heating rate was 0.6 K s^{-1}. CO desorption from blank Al_2O_3 was subtracted when plotting the dashed curve. Solid curve: TPD of CO into vacuum from 1.0-wt% Pt/Al_2O_3 with a Pt dispersion of 30–40%; the heating rate was 1 K s^{-1}. CO desorption from blank Al_2O_3 was negligible with respect to the solid curve.

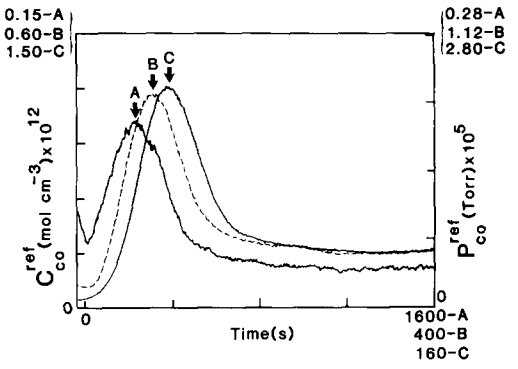

FIG. 4. Experimental measurements of the TPD of CO from 0.1-wt% Pt/Al_2O_3 with a CO/Pt ratio of 0.70. The temperatures at the peak maxima and the heating rates are (A) 337 K and 0.21 K s^{-1}, (B) 355 K and 0.93 K s^{-1}, and (C) 367 K and 2.4 K s^{-1}.

curve) to our results for desorption from intermediate-dispersion (30–40%) 1.0-wt% Pt/Al_2O_3 into vacuum (solid curve; the sample had been exposed to a series of pretreatments after preparation, the most recent was in H_2 at 673 K). Only the general shapes of the curves can be compared because of the vastly different experimental conditions (*1*). Higher CO concentrations were established over the Pt/Al_2O_3 during desorption into flowing He; as a result, the dashed curve is shifted to higher temperature with respect to the solid curve. We propose that the desorption-rate maximum present in both curves at about 390 K is related to the low-temperature peak we have observed and is associated with desorption of CO from the smallest Pt particles present in the samples.

Experiments were performed to determine the enthalpy of CO adsorption in the adsorption state that is associated with the low-temperature TPD peak. In Fig. 4, TPD curves are shown which were obtained at three different heating rates. The experiments were performed when the dispersion was 80% (CO/Pt = 0.70). Three experiments were performed at the two higher heating rates and two were performed at the lowest rate to ensure reproducibility. Note that the concentration, pressure, and time scales are different for each curve. The temperatures at the peak maxima, T_m, are (A) 337 K at a heating rate of 0.21 K s^{-1}, (B) 355 K at a rate of 0.93 K s^{-1}, and (C) 367 K at a rate of 2.4 K s^{-1}. For the case of adsorption equilibrium, a linear adsorption isotherm, and diffusional limitations during TPD from a porous adsorbent, Cvetanovic and Amenomiya (*15*) showed that the slope of a plot of $\ln(T_m^2/\beta)$ versus $(1/T_m)$ closely approximates $(\Delta H/R)$, where β is the heating rate, ΔH, is the enthalpy of adsorption, and R is the ideal gas constant. Our numerical simulations (*1*) showed that this analysis also holds for the case of a Langmuir isotherm when diffusional limitations are present, and Jones and Griffen (*16*) recently obtained this result analytically. Figure 5 shows a plot of $\ln(T_m^2/\beta)$ versus $(1/T_m)$ for the experiments shown in Fig. 4. The slope of the line indicates that an adsorption enthalpy of 74 ± 4 kJ mol^{-1} (18 ± 1 kcal mol^{-1}) is associated with the low-temperature CO desorption peak.

DISCUSSION

We have observed two types of CO desorption from Pt/Al_2O_3: CO desorption in a

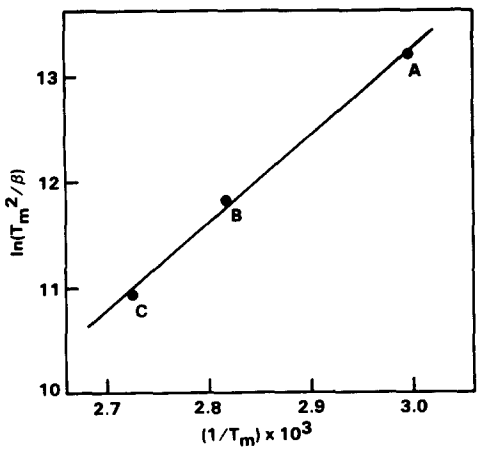

FIG. 5. Estimation of the enthalpy of adsorption of CO in the adsorption state which corresponds to the well-defined low-temperature TPD peak. The points were determined from the correspondingly labeled curves in Fig. 4. The T_m (K) is the temperature at which a peak maximum occurred at the heating rate β (K s^{-1}). The slope of the line multiplied by the ideal gas constant approximates the adsorption enthalpy, which we estimate to be 74 ± 4 kJ mol^{-1} (18 ± 1 kcal mol^{-1}).

well-defined low-temperature peak and CO desorption in a broad desorption band. The relative proportions of these two types of desorption changed with the CO/Pt ratio. As the CO/Pt ratio decreased, the fraction of CO that desorbed in the low-temperature peak decreased and the fraction of CO that desorbed in the broad desorption band increased. In the absence of poisoning, the CO/Pt ratio of a sample is proportional to the Pt dispersion and is inversely proportional to the average size of Pt particles in the sample, where we define the term "particle" to refer to one Pt atom as well as a three-dimensional aggregate of two or more Pt atoms. Thus, our results indicate that (1) the well-defined low-temperature peak is associated with adsorption and desorption of CO over very small Pt particles supported on transitional Al_2O_3, and (2) the broad desorption band is associated with adsorption and desorption of CO over larger Pt particles.

The range of particle size associated with the low-temperature peak can be estimated by considering curve 1 in Fig. 2. The Pt dispersion was 100% (CO/Pt = 0.92) when this experiment was performed. Consequently, there is only a narrow range over which the sizes of the Pt particles in the sample could have varied: Pt particles in which essentially all atoms are exposed contain at most 20 atoms and have a maximum diameter of about 1.1 nm (*13, 14, 17*). Although we have not made direct measurements of the particle sizes in our CO/Pt = 0.92 sample, Yao *et al.* (*10*) found that the particles present in their CO/Pt = 0.85 Pt/Al_2O_3 sample had sizes below the 1.0-nm detection limit of their transmission electron microscope. Since only two thirds of the CO desorbed in the low-temperature peak in curve 1, Fig. 2, we propose that the particles associated with the peak contain *fewer* than 20 Pt atoms and are *less* than 1.1 nm in diameter. Two-dimensional arrays ("rafts") of Pt atoms in which every Pt atom is both in contact with the support and exposed to the gas phase may additionally be associated with the low-temperature desorption peak.

The Pt particles associated with the low-temperature TPD peak chemisorb CO with a relatively uniform bond energy—evidence which further suggests that the particles are constrained to a narrow size range. Numerical simulations of these experiments, which we will report later, indicate that the peak can be fit fairly well with a Langmuir adsorption isotherm and a constant adsorption enthalpy. That is, a strongly coverage-dependent adsorption enthalpy is not required to fit the relatively narrow width of the peak.

The adsorption enthalpy associated with the low-temperature peak, 74 ± 4 kJ mol^{-1}, falls below the range of activation energies that have been measured for desorption of CO over various crystallographic planes of Pt metal. McCabe and Schmidt (*18*) report desorption activation energies ranging from 95 to 148 kJ mol^{-1} over several different crystal planes. McClellan *et al.* (*19*) report activation energies of 96 kJ mol^{-1} for desorption from the (111) terraces of the

Pt(321) surface and 151 kJ mol^{-1} for desorption from low-coordination "kink" sites on this surface. CO adsorption on Pt metal is not activated, so these desorption activation energies can be compared directly with the adsorption enthalpy we have estimated.

The CO–Pt bond energy associated with very small Pt particles that are supported on transitional Al_2O_3 may be lower than the bond energies associated with the surfaces of bulk Pt metal for one or both of the following reasons:

(1) the limited number of atoms in the very small particles may make the electronic structure and CO bonding properties of the particles different from those of the surfaces of bulk Pt metal, and/or

(2) the transitional Al_2O_3 support may influence the electronic structure and CO bonding properties of the very small Pt particles. For example, charge transfer from very small Pt particles to the support might reduce Pt–CO bond strengths by reducing donation of electron density from Pt into the $2\pi^*$ orbitals of CO upon adsorption.

One third of the CO that desorbed from the 100%-dispersion Pt in curve 1 of Fig. 2 desorbed in the broad desorption band. We propose that this CO desorbed from the largest Pt particles that would have been present in the sample, particles containing about 20 Pt atoms and having a diameter of about 1.1 nm. As the Pt dispersion decreased in Fig. 2, the shape of the broad desorption band changed: proportionately more CO desorbed at higher temperatures. This change in the shape of the band may have resulted from changes in the surface structures of the particles as they increased in size (*17*) and/or changes in the electronic structures of the particles as they increased in size.

The width of the broad desorption band indicates that a distribution of adsorption sites with different CO–Pt bond energies is associated with the larger Pt particles ($\geq$20 atoms, $\geq$1.1 nm) we are considering. This is not surprising when we consider that atoms on the surfaces of small (1–10 nm) metal crystallites are arranged in a distribution of different geometric configurations (*17*) and that CO–Pt bond energies have been found to vary widely over Pt single crystal surfaces with different crystallographic orientations. If one were to sum the TPD curves reported by McCabe and Schmidt (*18*) for CO desorption from a variety of Pt crystal planes, one would obtain a broad band not unlike that measured over intermediate-dispersion Pt/Al_2O_3. Further analysis is required before we can estimate the range of adsorption energies that is associated with the broad desorption band; however, our results do suggest that the particles associated with the broad band behave similarly to bulk Pt metal with respect to CO chemisorption.

Relatively weak adsorption of CO on small Al_2O_3-supported noble metal particles and relatively strong adsorption on larger particles have been reported by others. Rothschild and Yao (*7*) used infrared spectroscopy to study CO chemisorption over Pt/γ-Al_2O_3. Over a sample with a CO/Pt ratio of 0.83, they found that the infrared absorption band of CO could be removed by "outgassing" at 623 K for 30 min (no Pt particles larger than 1.0 nm were detected by electron microscopy in this sample). Over a sample with a CO/Pt ratio of 0.26, however, the CO band was only partially removed by "outgassing" at 723 K for 30 min (particle sizes between 1.0 and 5.5 nm were detected in this sample). Rothschild and Yao attributed their qualitative observation of weaker CO adsorption to stronger Pt–Al_2O_3 interactions (types unspecified) in the higher dispersion sample. If charge transfer from Pt to the support is such an interaction, then decreased charge donation from Pt into the antibonding $2\pi^*$ CO orbitals could result in a higher C–O stretching frequency over smaller Pt particles, other factors remaining equal. Rothschild and Yao reported a CO infrared absorption band maximum at 2060 cm^{-1} (at saturation coverage) over small Pt particles (<1.0 nm, "dispersed phase") and at 2050

cm^{-1} over larger Pt particles ("particulate phase"), results which appear to be consistent with this interpretation. However, the band maximum was at 2070 cm^{-1} over samples containing both small and large Pt particles ("dispersed + particulate phase"), a result which is not consistent with the first set of band positions. In contrast, we have observed the CO band at lower wavenumbers over our 0.1-wt%, 100%-dispersion sample (2062–2064 cm^{-1}) than over 1-wt%, 30%-dispersion Pt/Al_2O_3 (2068–2070 cm^{-1}). In addition to Pt–CO backbonding, charge donation from the 5σ orbital of CO to the metal upon adsorption contributes to the Pt–CO bond energy, and this contribution to the bonding may be affected by $Pt–Al_2O_3$ interactions. Thus, simple correlations between C–O stretching frequency, Pt–CO bond energy, and Pt particle size might not exist over Pt/Al_2O_3.

In another study with results which parallel ours, Ladas *et al.* (*8*) measured TPD of CO into vacuum from Pd particles supported on nonporous α-Al_2O_3. They measured CO desorption from two adsorption states—one with a CO adsorption energy estimated to be 125–145 kJ mol^{-1} and one with a CO adsorption energy estimated to be 100–125 kJ mol^{-1}. A sample with an average Pd particle size of 1.5 nm had proportionately more CO desorption from the low-energy adsorption state than a sample with an average Pd particle size of 5.9 nm.

Recently, Doering *et al.* (*9*) reported measurements of the TPD of CO into vacuum from Pt particles dispersed over flat mica surfaces. We think it valuable to discuss their results here although a direct comparison between our systems cannot be made since (1) the surface of mica (potassium/silica, roughly) may interact differently with small Pt particles than does Al_2O_3, and (2) somewhat different particle size ranges were considered in the two studies. Desorption curves measured over Pt with an average particle size of 1.6 nm in (*9*) showed two unresolved peaks: one at temperatures characteristic of desorption from Pt(111) planes and a smaller peak at higher temperatures which was ascribed to desorption from low-coordination Pt sites such as "steps" and "kinks." Note that the particles in this sample were larger than the Al_2O_3-supported particles that we associate with our low-temperature peak. Over larger particles in (*9*), desorption at high temperatures was reduced and desorption characteristic of Pt(111) planes predominated. This result is reasonable since the proportion of low-coordination Pt sites will decrease with particle size (*17*). By analogy, we predict that TPD curves obtained over very low dispersion Pt/Al_2O_3 will be characteristic of desorption from Pt(111) planes and will show less desorption at high temperatures when compared with the curves shown in Fig. 3 for intermediate-dispersion Pt/Al_2O_3.

CONCLUSIONS

The data presented here indicate that very small Pt particles (<20 Pt atoms, <1.1 nm diameter) that are supported on transitional Al_2O_3 chemisorb CO with a CO–Pt bond energy of 74 ± 4 kJ mol^{-1}. The data also indicate that larger transitional-Al_2O_3-supported Pt particles chemisorb CO more strongly on adsorption sites with a wide distribution of CO–Pt bond energies.

ACKNOWLEDGMENTS

We thank Edward J. Shinouskis for infrared spectroscopic studies of our samples.

REFERENCES

1. Herz, R. K., Kiela, J. B., and Marin, S. P., *J. Catal.* **73,** 66 (1982).
2. Foger, K., and Anderson, J. R., *Appl. Surf. Sci.* **2,** 335 (1979).
3. Komers, R., Amenomiya, Y., and Cvetanoic, R. J., *J. Catal.* **15,** 293 (1969).
4. Cvetanovic, R. J., and Amenomiya, Y., *Catal. Rev.* **6,** 21 (1972).
5. Hoang-Van, C., Ghorbel, A., Pommier, B., and Teichner, S. J., *Bull. Soc. Chim. Fr.* **1976,** 355 (1976).
6. Miura, H., and Gonzalez, R. D., *J. Phys. Chem.* **86,** 1577 (1982).
7. Rothschild, W. G., and Yao, H. C., *J. Chem. Phys.* **74,** 4186 (1981).

8. Ladas, S., Poppa, H., and Boudart, M., *Surf. Sci.* **102,** 151 (1981).
9. Doering, D. L., Poppa, H., and Dickinson, J. T., *J. Vac. Sci. Technol.* **20,** 827 (1982).
10. Yao, H. C., Sieg, M., and Plummer, H. K., Jr., *J. Catal.* **59,** 365 (1979).
11. Doering, D. L., Poppa, H., and Dickinson, J. T., *J. Catal.* **73,** 104 (1982).
12. Hair, M. L., "Infrared Spectroscopy in Surface Science," p. 158. Dekker, New York, 1967.
13. Wilson, G. R., and Hall, W. K., *J. Catal.* **17,** 190 (1970).
14. Dorling, T. A., and Moss, R. L., *J. Catal.* **7,** 378 (1967).
15. Cvetanovic, R. J., and Amenomiya, Y., "Advances in Catalysis," Vol. 17, p. 103. Academic Press, New York, 1967.
16. Jones, D. M., and Griffin, G. L., *J. Catal.,* **80,** 40 (1983).
17. vanHardeveld, R., and Hartog, F., *Adv. Catal.* **22,** 75 (1972).
18. McCabe, R. W., and Schmidt, L. D., *Surf. Sci.* **66,** 101 (1977).
19. McClellan, M. R., Gland, J. L., and McFeeley, F. R., *Surf. Sci.* **112,** 63 (1981).